PHYSICAL REVIEW B **104**, 224432 (2021)

Tuning the magnetocaloric effect by optimizing thickness-induced three-dimensional strain states

Samir Kumar Giri,[1,*] Wasim Akram,[2,*] Manisha Bansal,[2] and Tuhin Maity[2,†]
[1]*Kharagpur College, Kharagpur, Paschim Medinipur, West Bengal 721305, India*
[2]*School of Physics, Indian Institute of Science Education and Research Thiruvananthapuram, Thiruvananthapuram, Kerala 695551, India*

(Received 6 May 2021; revised 26 November 2021; accepted 6 December 2021; published 28 December 2021)

The effect of a three-dimensional strain state on the magnetocaloric properties of epitaxial $La_{0.8}Ca_{0.2}MnO_3$ (LCMO) thin films grown on two types of substrates, $SrTiO_3$ (001) (STO) and $LaAlO_3$ (001) (LAO), has been studied as a function of film thickness within the range of 25–300 nm. The STO substrate imposes an in-plane tensile biaxial strain, while the LAO substrate imposes an in-plane compressive biaxial strain. The in-plane biaxial strain on LCMO by the STO substrate gets relaxed more rapidly than that by the LAO substrate but both LCMO/STO and LCMO/LAO show a maximum entropy change ($\Delta S_{\max}$) of $\sim$12.1 J $Kg^{-1}K^{-1}$ (76.33 mJ $cm^{-3}K^{-1}$) and $\sim$3.2 J $Kg^{-1}K^{-1}$ (20.18 mJ $cm^{-3}K^{-1}$), respectively, at a critical thickness of 75 nm (at 6 T applied magnetic field). LCMO/LAO is found to exhibit a wider transition temperature region with full width at half maxima (FWHM) $\sim$40 K of the $\frac{dM}{dT}$ vs T curve compared to LCMO/STO with FWHM $\sim$33 K of that curve. This broadening of the transition region indicates that the table-like magnetocaloric effect (MCE) is attainable by changing the strain type. The maximum relative cooling power, $\sim$361 J Kg^{-1} (2277 mJ cm^{-3}) of LCMO/STO and $\sim$339 J Kg^{-1} (2138.5 mJ cm^{-3}) of LCMO/LAO, is also observed at the thickness $\sim$75 nm. The Curie temperature varies with the thickness exploring the variation of ferromagnetic interaction strength due to strain relaxation. The film thickness and substrate induced lattice strain are proved to be the significant parameters for controlling MCE. The highest MCE response at a particular thickness shows the possibility of tuning MCE in other devices by optimizing thickness.

DOI: 10.1103/PhysRevB.104.224432

I. INTRODUCTION

Depletion of energy resources is pushing the scientific community to materialize energy-efficient and environmental friendly technologies. To sustain the nature and the running demands alongside, low power refrigeration or cooling at both macro- and microscale has been proved to be one of the future energy saving innovations [1–4]. Existing cooling techniques include absorption and adsorption refrigerators, thermoelectric cooling, thermoacoustic refrigerators, ejector refrigeration systems, magnetocaloric (MC) refrigeration, etc. [5,6]. Among these, magnetocaloric effect (MCE) is the most promising candidate due to its efficiency and environmentally friendly approach. Use of thermal effects induced by the application of magnetic field to produce efficient cooling, popularly known as MCE, has gained recognition among the researchers [7–9]. Room temperature cheap and efficient MC devices lead to potent energy safeguarding household and industrial applications outperforming conventional cooling or refrigeration techniques [10]. However, only a few materials can be used for MC applications due to the complexity involved in studying the coupled magnetic and structural parameters of the system [11–13]. Materials should have high MC constant, wide range of operating temperature, low hysteresis loss, low specific heat, high thermal conductivity, etc., to produce large MCE response, which is challenging as of significant technological importance. Recent material research shows possible improvement in the MCE efficiency concomitant with challenges like fabrication complexity, less resistance to corrosion, poor conductivity, etc. [2,14,15]. Different alloys (e.g., iron based alloy $Gd_5Ge_{1.9}Si_2Fe_{0.1}$) [16] and composites [e.g., La(Fe, Si)$_{13}$Hy/In] [2] showed potential to overcome such deficiencies, henceforth improving the performance of MCE based magnetic refrigeration or cooling.

Moreover, most research activities on MCE are limited to bulk materials since the studies on thin films are more complex due to the intricacies involved in their fabrication and study. But the industries especially for micro- and nanoscale devices are in a huge demand of thin film based MCE because of their high efficiency, less space consumption, flexibility, larger specific surface area for higher exchange of heat, etc. [17,18]. Interestingly, epitaxial thin films show several fascinating phenomena including colossal magnetoresistance (CMR) due to the additional strain constraints [19,20], which are of particular importance to determine their physical properties [21–24]. The giant MCE has been observed in the CMR based epitaxial manganite systems like $La_{0.67}Sr_{0.33}MnO_3$ (LSMO)/$BaTiO_3$ (BTO) (with the entropy change per unit field, $\Delta S_M/\mu_0\Delta H = 1.95$ J $Kg^{-1}K^{-1}T^{-1}$) [25], $La_{0.7}Ca_{0.3}MnO_3$/BTO [$\Delta S_M/\mu_0\Delta H = -0.7$ J $Kg^{-1}K^{-1}T^{-1}$ near Curie temperature of $La_{0.7}Ca_{0.3}MnO_3$ (intrinsic) and -9.0 J $Kg^{-1}K^{-1}T^{-1}$ due to structural phase transition of BTO (extrinsic)] [26], where the substrate induced strain influences the temperature dependent magnetic properties of the CMR materials resulting in adiabatic thermal process [27–29].

---

[*] These authors contributed equally to this work.
[†] tuhin@iisertvm.ac.in

This substrate induced strain may be compressive (tensile) depending upon larger (smaller) lattice parameter (a^P) of the epitaxial film than that of the substrate [22,30,31], which results in decrease (increase) of the Mn-O bond length as well as altering the Mn-O-Mn bond angle [22]. Generally, under a tensile strain, ferromagnetism due to double exchange (DE) interaction gets weakened because of the reduction in e_g electron transfer integral, $t_\alpha = t_\alpha^\star \sin(\phi/2)$, where $t_\alpha^\star$ is the bare transfer integral and ϕ is the Mn-O-Mn bond angle [32], whilst under compressive strain, DE interaction is strengthened to give rise to stronger ferromagnetism [33]. So, strain is a crucial parameter to determine the strength of the ferromagnetic interaction. In particular, the dominant ferromagnetic exchange favors a large spin ground state enhancing the large field dependence of entropy change (ΔS_M) and hence improving MCE [34–36]. But, the relation of the strain with such ΔS_M has not been addressed yet according to our knowledge. Nevertheless, strain has the potential of greatly affecting the transition temperatures as well. The tensile (compressive) strain decreases (increases) the Curie temperature (T_C) [32,33] by weakening (strengthening) the DE interaction. Contrary to this general expectation, several reports [37–39] were able to convey that the tensile strain also drives up T_C, while the compressive strain reduces it [40]. Therefore, a clear approach is essential in this subject.

Here, we investigate the evolution of strain states on MCE in the epitaxial $La_{0.8}Ca_{0.2}MnO_3$ (LCMO) thin films grown on STO and LAO substrates which give rise to tensile and compressive strain, respectively. An entropy change for different temperatures is studied with varying t. By optimizing t and hence substrate induced lattice strain, a large entropy change of $\Delta S_M = 2\ \mathrm{J\,Kg^{-1}K^{-1}T^{-1}}$ ($12.6\ \mathrm{mJ\,cm^{-3}K^{-1}T^{-1}}$) in epitaxial $La_{0.8}Ca_{0.2}MnO_3$ is achieved, which is larger than the bulk value ($\Delta S_M = 0.9\ \mathrm{J\,Kg^{-1}K^{-1}T^{-1}}$ for $La_{0.67}Ca_{0.33}MnO_3$ [41]). The maximum value of entropy change ($\Delta S_{\max}$) is examined and proposed to be a well-known function of t. Further, a correlation between the MCE and t dependent strain relaxation is found. Besides, the transition temperatures are observed to vary with t anomalously and its maxima at a particular thickness is attributed to the strain relaxation. The convenient adjustment of T_C by varying t widens the way of achieving room temperature MCE in epitaxial thin films. Generally, for cooling applications, distributed magnetic ordering temperature is highly desiderated as it brings on table-like MCE [42,43], which is the basis of ideal Ericsson-cycle based magnetic refrigeration [42]. Here, the broadening of the transition region for LCMO/LAO rather than that of the LCMO/STO suggests the possibility of acquiring table-like MCE by changing the strain type. To compare the viability of these LCMOs grown on STO and LAO as an efficient refrigerant, the relative cooling power (RCP) is calculated and studied with varying t and magnetic field (H). The RCPs associated with the first order magnetic phase transition (FOMPT) and the second order magnetic phase transition (SOMPT) have proved to be advantageous in different ways. Finally, a way to choose the right substrate is suggested with respect to the need for an optimum working temperature span as well as ΔS_M value.

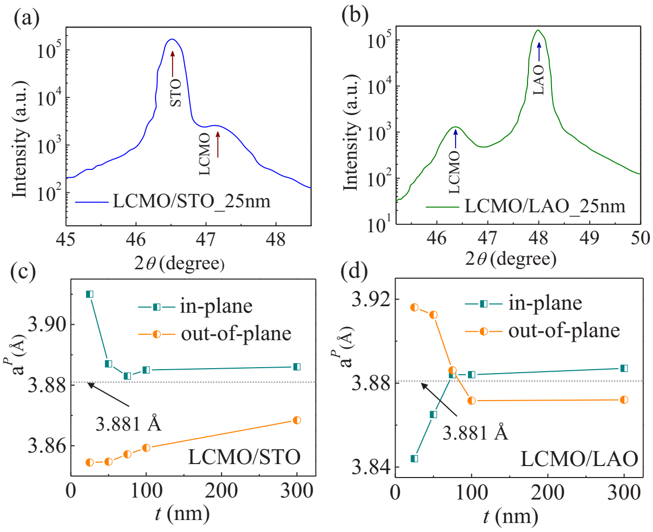

FIG. 1. (a),(b) Grazing incidence XRD scans of 25 nm LCMO films grown on STO and LAO substrates, respectively. Panels (c) and (d) show the variation of lattice parameters as a function of t of LCMO/STO and LCMO/LAO, respectively.

II. EXPERIMENTAL METHOD

The epitaxial LCMO thin films were grown by pulsed laser deposition (PLD) technique from a stoichiometric target at 750 °C with an oxygen pressure of 300 mTorr and an estimated laser energy density of $\sim 3.5\ \mathrm{J\,cm^{-2}}$ with a repetition rate of 5 Hz. Two different types of single crystal substrates, i.e., LAO (001) ($a^P \sim 3.79$ Å) and STO (001) ($a^P \sim 3.905$ Å), were used to attain two different types of lattice mismatch for the growth of LCMO thin films. The thicknesses of the films were varied from 25 nm to 300 nm in order to correlate the strain relaxation process with MCE. The composition of the film with target was confirmed from wavelength dispersive x-ray spectroscopy within experimental error. Structural characterization was carried out using a four-circle x-ray diffractometer. Figures 1(a) and 1(b) show XRD scans of 25 nm LCMO films grown on STO and LAO substrates, respectively. The out-of-plane and in-plane lattice parameters were determined by normal $\theta - 2\theta$ and grazing incidence diffraction (GID) scans at room temperature, respectively. The variation of in-plane and out-of-plane lattice parameters with respect to t for the two different substrates is shown in Figs. 1(c) and 1(d). The bulk value of LCMO lattice parameter (3.881 Å) is obtained from the target pellet. Temperature-dependent magnetizations of all LCMO thin films were measured, in order to explore the effect of 3D strain states on magnetic properties. Magnetization measurements were carried out using a SQUID magnetometer in the temperature range 5–300 K and field range of 6 T. The temperature dependent zero field cooled (ZFC) magnetization (M) vs temperature (T) of all the films are taken at $H = 5$ mT. For the slow magnetic field scan, 0.01 T per minute ramp rate was used in SQUID to consider all of the magnetization process as quasiequilibrium and isothermal.

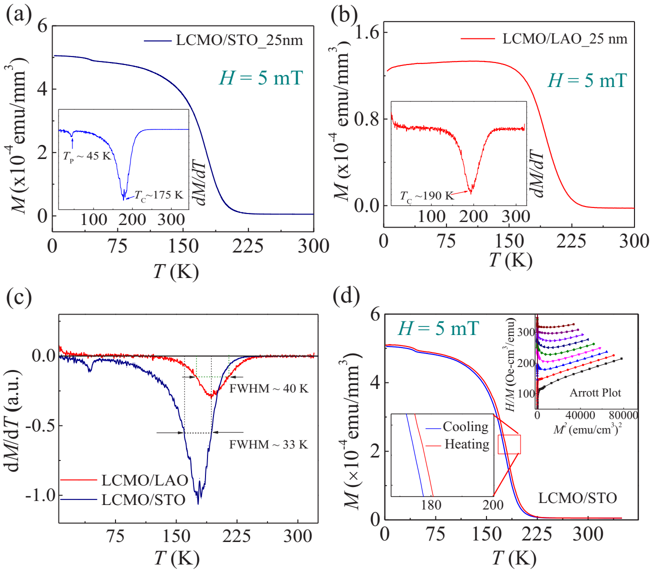

FIG. 2. (a),(b) M vs T curves of 25 nm LCMO/STO and LCMO/LAO, respectively, under 5 mT magnetic field. Inset figures show the $\frac{dM}{dT}$ vs T curves and corresponding T_C. (c) Broadening of the transition region for LCMO/STO compared to LCMO/LAO. (d) Hysteresis between the warming up and cooling down cycle of magnetization for LCMO/STO under 5 mT field. Right inset shows the Arrott plot around T_C.

III. RESULTS AND DISCUSSION

It is evident from the XRD scans that the epitaxially grown LCMO thin films are subjected to two distinct strain states on LAO and STO substrates. In Figs. 1(c) and 1(d), the in-plane lattice parameters of the LCMO thin films obtained from grazing incidence x-ray diffraction (GID) at room temperature are found to be deviated from that of the substrates to the bulk value (3.881 Å) with the increase in t. Rao *et al.* [44] have previously discussed the variation of the 3D strain state with respect to t in detail. The LAO substrate ($a^P \sim 3.79$ Å) imposes an in-plane compressive strain with lattice mismatch -2.34%, while the STO substrate ($a^P \sim 3.905$ Å) imposes a corresponding tensile strain with a lattice mismatch $+0.62\%$ on the films.

The temperature dependence of the in-plane magnetization of LCMO/STO and LCMO/LAO is shown in Figs. 2(a) and 2(b), respectively. The transition temperatures are obtained from the extrema of $\frac{dM}{dT}$ vs T curves [insets of Figs. 2(a) and 2(b)]. The full width at half maximum (FWHM) of a $\frac{dM}{dT}$ vs T curve around T_C for LCMO/LAO (~40 K) is larger than that of the LCMO/STO (~33 K) [Fig. 2(c)], elucidating the broadening of the transition region for the former compared to the latter. Along with the absence of any thermal hysteresis in MT curve for LCMO/LAO, this broadening suggests the probability of SOMPT, while the thermal hysteresis in MT curve for LCMO/STO [Fig. 2(d)] between field cooling and field heating indicates the FOMPT at transition temperature [45]. This is confirmed by the Arrot plot [inset of Fig. 2(d)] and Banerjee criterion [46]. According to the Banerjee criterion, the slope of the H/M vs M^2 plot should be negative for FOMPT. In the present investigation for LCMO/STO, the observed negative slope of the Arrott plot around T_C is the clear indication of FOMPT.

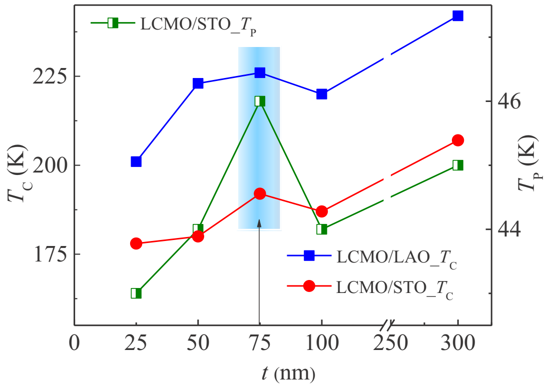

FIG. 3. T_C and T_P vs t plot for LCMO/LAO and LCMO/STO.

Further, in addition to T_C, the $\frac{dM}{dT}$ vs T curve of LCMO/STO shows a dip at T_P (~43 K–46 K) to be the freezing temperature [47–49], below which the spin-glass-like state is formed in LCMO/STO. However, this is absent for LCMO/LAO due to stronger ferromagnetic interaction arising from compressive strain. Under compressive strain, the DE interaction is strengthened, inducing stronger ferromagnetism and removing the disorder of the spin-glass-like state [48]. Hence T_P is absent in LCMO/LAO. But the tensile strain in LCMO/STO weakens DE interaction, giving rise to weaker ferromagnetism. As a consequence, a spin-glass-like state can be formed easily towards the lower temperature region giving rise to T_P in LCMO/STO.

For comparison, T_C and T_P of the epitaxial LCMO films are plotted as a function of t in Fig. 3. LCMO/LAO shows higher T_C compared to LCMO/STO of the same t due to persistence of stronger ferromagnetism below transition temperature T_C under compressive strain [50]. However, the transition temperatures T_C and T_P vary nonmonotonously with the strain relaxation on increasing t below 100 nm thickness. Both of them at first go on increasing for up to 75 nm thickness and then decrease. This can be explained as dominating behavior of the ferromagnetic (FM) phase up to 75 nm thickness, which has been discussed later. At 300 nm thickness both T_C and T_P are higher which is usual for thin film [51,52]. The increase in T_C for tensile strain relaxation up to $t \sim 75$ nm originates from the strengthening of DE interaction due to Mn-O bond length reduction [32]. However, the compressive strain induced ferromagnetism in the LCMO system observed here is in contrast as T_C was supposed to be decreased on strain relaxation due to weakening of DE interaction. So, this anomaly needs to be understood.

To understand this, two effects should be taken into consideration as the result of the in-plane Mn-O bond length elongation (contraction)—one is the decrease (increase) of the e_g electron transfer integral as mentioned before and another is electron localization in the $d_{x^2-y^2}$ orbital [22] due to in-plane $d_{x^2-y^2}$-orbital stabilization [32], which can enhance the ferromagnetism and increase T_C. In particular, Mn^{3+} ions in $LaMnO_3$ are already known to be arranged in an A type planar antiferromagnetic structure consisting of oppositely aligned

FM {001} planes [53]. Hence in-plane Mn^{3+} ions interact ferromagnetically with each other. When $LaMnO_3$ is doped with divalent Ca^{2+} ions, they replace some of the trivalent La^{3+} ions and form a mixed valence state in Mn ions (Mn^{3+} and Mn^{4+}) [54]. The Mn^{3+} and Mn^{4+} ions interact with each other ferromagnetically through DE interaction mediated by O-2p orbital electrons [55]. The spacing between Mn^{4+} and Mn^{3+} gets increased under tensile strain giving rise to reduction [32] in the e_g orbital electron transfer integral and weakening ferromagnetism due to DE interaction and the reverse case happens for the compressive strain. But, at the same time, due to elongation of the in-plane Mn-O bond length, the overlapping between the lobes of the in-plane Mn-3d orbitals and O-2p orbitals gets decreased [56], giving rise to lower Coulomb repulsion and favoring the in-plane orbital electron localization [22], which in turn induces ferromagnetism. So, due to the competition between these two effects, the practical behavior depends on the dominant effect or possibly a mixed effect. For tensile strain, the reduction in DE interaction dominates over orbital electron localization, whereas the latter one dominates over the first one for compressive strain and, due to compressive strain relaxation, the in-plane orbital electrons are getting localized to give rise to stronger ferromagnetism. Above 75 nm thickness, T_C for each sample starts to fall from the maximum value indicating that the dominating behavior is not always the same throughout the strain relaxation process. The viability of these epitaxial LCMOs as the core refrigeration system can be investigated by a comparative study of the MCE produced by these. The MCE is parametrized by the isothermal magnetic entropy change [$(\Delta S_M)_{\text{iso}}$] and/or adiabatic temperature change (ΔT_{ad}) of a magnetic material under the variation of H [18]. Most of the research reports publish $(\Delta S_M)_{\text{iso}}$ data instead of ΔT_{ad} for the former being easily measurable with standard magnetometers, but ΔT_{ad} measurement having some technical difficulty at the micro- and nanoscale due to uncertainty of adiabatic procedure and occurrence of the rapid thermal diffusion from the studied micro/nanostructure towards a heat/cold sink [6,18]. The isothermal magnetic entropy change $\Delta S_M(H)$ of a magnetic material on application of magnetic field H at temperature T can be written from Maxwell's thermodynamic relation $(\frac{\partial S}{\partial H})_T = (\frac{\partial M}{\partial T})_H$ as [26]

$$\begin{aligned}\Delta S_M(T,H) &= S_M(T,H) - S_M(T,0)\\ &= \int_0^H \left(\frac{\partial M}{\partial T}\right)_H dH.\end{aligned} \tag{1}$$

This expression ensures the maximum magnetic entropy change around the transition temperature due to switching in magnetic ordering and rapid change of magnetization. However, Eq. (1) is not directly used here to calculate $|\Delta S_M|$ values. Due to discrete interval of temperature and applied magnetic field used for magnetization measurements, Eq. (1) is approximated to

$$|\Delta S_M| = \sum \frac{(M_n - M_{n+1})}{(T_{n+1} - T_n)} \Delta H_n, \tag{2}$$

where M_n and M_{n+1} are the magnetization values measured in a field H at temperatures T_n and T_{n+1}, respectively [57–59]. Evidently, the area between two consecutive isothermal MH curves [insets of Figs. 4(c) and 4(d), shown for 75 nm thickness only] divided by the temperature interval $\Delta T (= T_{(n+1)} - T_n)$ gives the value of $|\Delta S_M|$ [58]. The calculated $|\Delta S_M|$ values are then associated with the averages of the temperatures $T_{(n+1)}$ and T_n i.e., $\frac{(T_{(n+1)}+T_n)}{2}$, and plotted (Fig. 4). In this work, the isothermal M was obtained in emu cm^{-3} on varying H and converted to emu/g by dividing it with the density (∼6.3084 g cm^{-3}). Using the obtained values of M in emu/g, $|\Delta S_M|$ values were calculated in J $kg^{-1}K^{-1}$. The bulk LCMO density was used for unit conversion as under tensile or compressive strain volume does not change significantly due to volume conservation keeping the density almost constant.

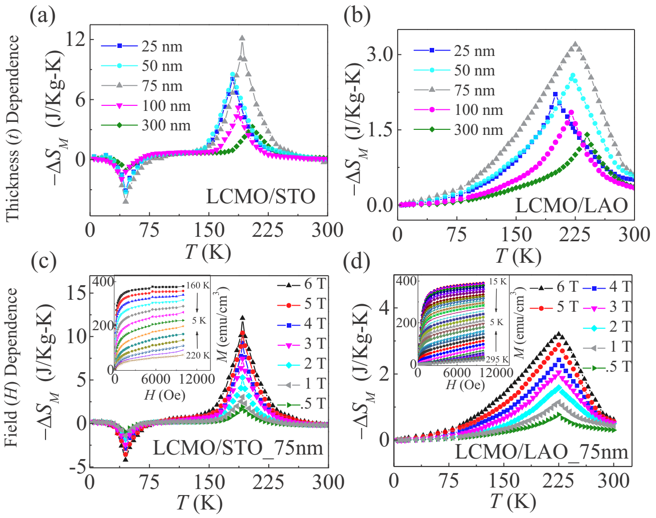

FIG. 4. $-\Delta S_M$ vs T curve for (a) LCMO/STO and (b) LCMO/LAO on varying t from 25 nm to 300 nm. Panels (c) and (d) are $-\Delta S_M$ vs T curve for LCMO/STO and LCMO/LAO, respectively, at $t \sim 75$ nm on varying H from 6 T to 0.5 T. Insets of (c) and (d) show the corresponding isothermal MH curves measured in a 5 K temperature interval.

From the isothermal MH curves [insets of Figs. 4(c) and 4(d)], it is seen that the saturation magnetization (M_S) of 75 nm LCMO/STO thin film at 180 K is nearly 280 emu cm^{-3}, while for 75 nm LCMO/LAO it is 55 emu cm^{-3}. It indicates that the compressive strain drastically changes the M_S, which is well in agreement with Ref. [60]. The M_S of the bulk is nearly 378 emu cm^{-3} at 181 K [61]. So, for thin films, M_S is generally lower than that of the bulk. However, it is evident from Eq. (2) that $|\Delta S_M|$ depends on $\frac{\partial M}{\partial T}$ rather than M_S. For LCMO/STO, this value is a few times larger than that of the LCMO/LAO. Hence LCMO/STO shows higher $|\Delta S_M|$ value near the transition temperature.

Here, $-\Delta S_M$ derived from the Maxwell equation show a negative peak (i.e., inverse MCE) around T_P (for LCMO/STO) [Figs. 4(a) and 4(c)] and a positive peak (i.e., normal MCE) around T_C (Fig. 4, for LCMO/STO and LCMO/LAO both), respectively. Both peaks increase with increasing H [Figs. 4(c) and 4(d)]. For LCMO/STO, the maximum value of $-\Delta S_M$ [+12.1 J $Kg^{-1}K^{-1}$ (+76.33 mJ $cm^{-3}K^{-1}$)] at T_C is almost three times larger in magnitude than at T_P [$-\Delta S_M \sim -4.2$ J $Kg^{-1}K^{-1}$ (−26.5 mJ $cm^{-3}K^{-1}$)] for $\mu_0 H = 6$ T and $-\Delta S_M$ remains

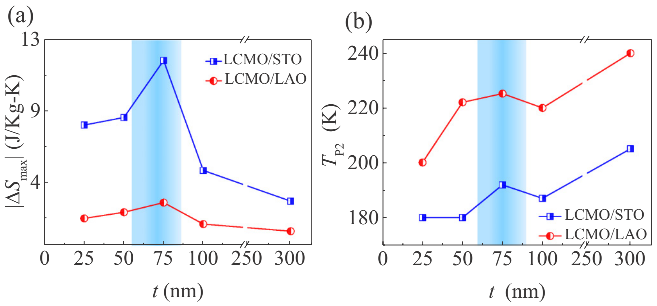

FIG. 5. (a) Plot of $|\Delta S_{\max}|$ against t for LCMO/STO and LCMO/LAO. (b) Temperature at $|\Delta S_{\max}|$ (T_{P2}) vs t plot.

in a narrow temperature regime around T_C due to FOMPT while, for LCMO/LAO, it gets broadened over a wide temperature range due to the suppression of FOMPT with the maximum value of $+3.2\ \mathrm{J\,Kg^{-1}K^{-1}}$ ($+20.18\ \mathrm{mJ\,cm^{-3}K^{-1}}$). Interestingly, $|\Delta S_M|$ changes due to variation of strain type on different substrates and strain amount of different t [Fig. 5(a)]. To make sure that the temperature for maximum entropy change (T_{P2}) and the transition temperature (T_C) follow a similar trend, T_{P2} is plotted against t [Fig. 5(b)].

At 75 nm thickness both the $|\Delta S_{\max}|$ and T_{P2} show maxima and, to investigate this anomalous behavior, we plotted the JT distortion (ϵ_{JT}) and in-plane biaxial strain ($\epsilon_{XX} = \epsilon_{YY}$) against t [Figs. 6(a) and 6(b)]. Both are decaying exponentially following the equation

$$\epsilon = \epsilon^{\star} e^{-\frac{t}{t_0}} + \epsilon_0, \tag{3}$$

with the fitting parameters $\epsilon^{\star}$, ϵ_0, and t_0 [for ϵ_{JT} curve (dark cyan colored) of LCMO/STO [Fig. 6(a)] and LCMO/LAO [Fig. 6(b)], $\epsilon^{\star} = -1.92\%$ and 4.42%, $\epsilon_0 = -0.42\%$ and -0.3%, and $t_0 = 25.5$ nm and 30.9 nm, respectively; for ϵ_{XX} curve (red colored) of LCMO/STO [Fig. 6(a)] and LCMO/LAO [Fig. 6(b)], $\epsilon^{\star} = 3.71\%$ and -2.25%, $\epsilon_0 = 0\%$ and 0%, and $t_0 = 15.5$ nm and 30 nm, respectively], where t_0 is the thickness at which the strain drops to $1/e$ times its maximum value and indicates how fast the strain gets relaxed with increasing t. The product $(\epsilon_{XX} \times \epsilon_{JT})$ which is the combined effect on $|\Delta S_{\max}|$ by in-plane strain and JT distortion also follows a similar exponential decay curve:

$$(\epsilon_{XX} \times \epsilon_{JT}) = (\epsilon_{XX} \times \epsilon_{JT})^{\star} e^{-\frac{t}{t_0}}, \tag{4}$$

with the fitting paramaters $(\epsilon_{XX} \times \epsilon_{JT})^{\star} = -0.075\%$ and -0.052%, and $t_0 = 11.5$ nm and 20 nm for LCMO/STO [Fig. 6(c)] and LCMO/LAO [Fig. 6(d)], respectively. All the strain components mentioned here and their products for LCMO/STO decay more rapidly than those of the LCMO/LAO, respectively.

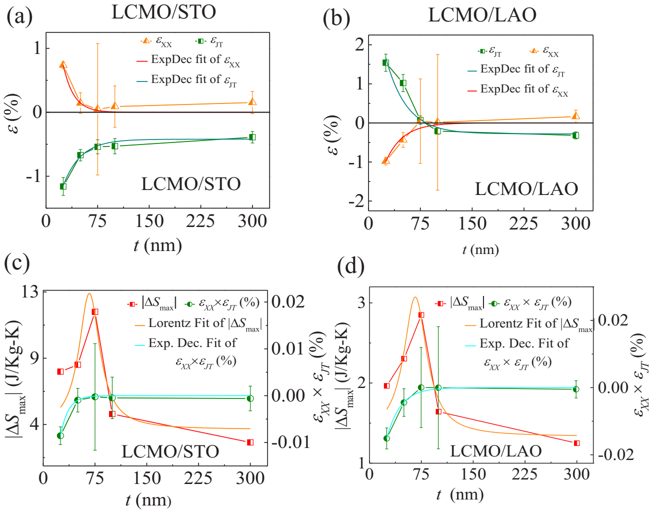

FIG. 6. In-plane biaxial strain (ϵ_{XX}) relaxation and decaying of Jahn-Teller distortion (ϵ_{JT}) of (a) LCMO/STO and (b) LCMO/LAO. The vertical error bars are standard deviation. (c),(d) $\epsilon_{XX} \times \epsilon_{JT}$ and $|\Delta S_{\max}|$ vs t plot of LCMO/STO and LCMO/LAO, respectively.

For the given range, the t dependence of $|\Delta S_{\max}|$ can be well fitted with the Lorentz function,

$$|\Delta S_{\max}| = (|\Delta S_{\max}|_0) + \frac{a}{b^2 + (t - t_1)^2}, \tag{5}$$

with highest value at $t = t_1$ yielding the fitting parameters $|\Delta S_{\max}|_0 = 4.14\ \mathrm{J\,Kg^{-1}K^{-1}}$ ($26.1\ \mathrm{mJ\,cm^{-3}K^{-1}}$), $a = 3124.23\ \mathrm{J\,Kg^{-1}nm^2}$ ($19.71\ \mathrm{J\,cm^{-3}K^{-1}nm^2}$), $b = 18.4$ nm, and $t_1 = 66.8$ nm for LCMO/STO [Fig. 6(c)] and $(|\Delta S_{\max}|)_0 = 1.49\ \mathrm{J\,Kg^{-1}K^{-1}}$ ($9.4\ \mathrm{mJ\,cm^{-3}K^{-1}}$), $a = 805.15\ \mathrm{J\,Kg^{-1}nm^2}$ ($5.08\ \mathrm{J\,cm^{-3}K^{-1}nm^2}$), $b = 20.3$ nm, and $t_1 = 66.3$ nm for LCMO/LAO [Fig. 6(d)]. This explains the continuous variation of $|\Delta S_{\max}|$ as a function of t with respect to $|\Delta S_{\max}|_0$ showing a maximum value at $t = t_1$ (∼66 nm ± 5 nm), which is almost the same for both LCMO/STO and LCMO/LAO. The maximum value of $|\Delta S_{\max}|$ arises due to the strongest FM interaction at $t = t_1$. Here (experimentally at $t \sim 75$ nm) the product of in-plane biaxial strain and JT distortion decays to almost zero giving rise to strongest FM interaction at that particular t, which favors the large spin ground state enhancing $|\Delta S_{\max}|$ value [34–36]. Certainly more data points could give precise value of t_1 by reducing the deviation of the parameters.

Generally, the first order transition materials (FOTM) undergo larger magnetic entropy change (ΔS_M) with the smaller working temperature span (WT span) than the second order transition materials (SOTM) and exhibit temperature dependent magnetic hysteresis, which diminishes the energy efficiency of the magnetocaloric materials [68]. So, confusion may arise when figuring out the suitability in cooling application between FOTM with larger ΔS_M but smaller WT span and SOTM with smaller ΔS_M but larger WT span. To overcome this, instead of focusing only on WT span or only on ΔS_M, the net heat extracted in a cooling cycle known as RCP is calculated [68]. Three methods are used here to calculate RCP. The first method is the Wood and Potter method [69,70], by which RCP is defined by

$$\text{RCP-1} = \Delta S_M(\max) \times \delta T_{FWHM}, \tag{6}$$

where $\Delta S_M(\max)$ is the maximum magnetic entropy change and $\delta T_{FWHM} = T_{\mathrm{hot}} - T_{\mathrm{cold}}$. T_{hot} and T_{cold} are the temperatures of the hot and cold end of the refrigeration cycle and

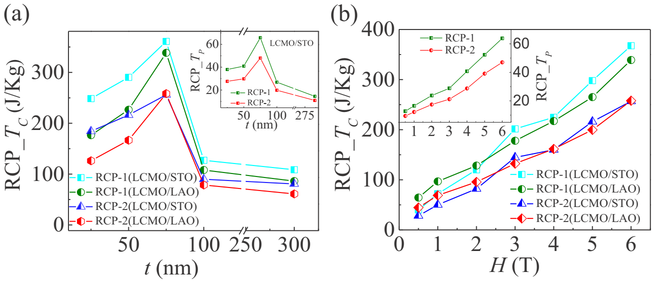

FIG. 7. RCP for LCMO/STO and LCMO/LAO calculated around T_C as a function of (a) t and (b) H. Inset figures show the RCPs of LCMO/STO calculated around T_P as a function of t and H, respectively.

these are essentially the upper and lower temperatures, respectively, at the half maxima of $\Delta S_M(T)$ vs T curve. δT_{FWHM} is considered as the working temperature range following the protocol as ΔS_M almost vanishes beyond this temperature range [71,72]. The second method is the area under the ΔS_M vs T curves taking T_{cold} and T_{hot} as the lower and upper limit of integration, respectively [1]. Here again $T_{\text{hot}} - T_{\text{cold}} = \delta T_{FWHM}$. So,

$$\text{RCP-2} = \int_{T_{\text{cold}}}^{T_{\text{hot}}} \Delta S_M(T, H_{\max})\, dT \ [1], \tag{7}$$

where $H_{\max}$ is the maximum value of the applied field. The third method is the maximization of the product ΔS_M and ΔT in the $\Delta S_M(T)$ vs T curve [69,73], i.e.,

$$\text{RCP-3} = [\Delta S_M(T) \times \Delta T]_{\max}. \tag{8}$$

We obtain large RCP-1 values, i.e., 361 J Kg^{-1} (∼2277 mJ cm^{-3}) of LCMO/STO and ∼339 J Kg^{-1} (∼2138.5 mJ cm^{-3}) of LCMO/LAO; RCP-2 values ∼255 J Kg^{-1} (∼1608 mJ cm^{-3}) of LCMO/STO and ∼258 J Kg^{-1} (1627 mJ cm^{-3}) of LCMO/LAO and RCP-3 values ∼191 J Kg^{-1} (∼1205 mJ cm^{-3}) of LCMO/STO and ∼169 J Kg^{-1} (1066 mJ cm^{-3}) of LCMO/LAO at $H = 6$ T for $t \sim 75$ nm. The estimated values of RCP-1 and RCP-2 near T_C as a function of t and H are plotted in Figs. 7(a) and 7(b), respectively. Insets of Fig. 7 show the RCPs around T_P for LCMO/STO.

It can be observed that, for both the temperature regimes, the value of RCP linearly increases with increasing H and has the largest value at $t \sim 75$ nm. In practical cooling applications, the material in the same refrigeration cycle with higher RCP is preferred as it would confirm the transport of a greater amount of heat in an ideal refrigeration cycle. To make the applicability of our results, i.e., to make the LCMO thin film as a magnetic refrigerant, $|\Delta S_{\max}|$ and the values of RCPs, i.e., RCP-1 and RCP-2, are determined in this present study and they are compared in Table I with several other magnetic refrigerants reported earlier in the literature. It is clearly evident from Table I that the obtained peak values of $|\Delta S_{\max}|$ and the RCPs at a critical t of 75 nm in our work are also comparable with other listed magnetic refrigerants.

TABLE I. Comparison of $|\Delta S_{\max}|$ (in J Kg^{-1}K^{-1}) and RCPs (in J Kg^{-1}) of different MC materials.

Compound	$\lvert\Delta S_{\max}\rvert$ [a]	RCP-1[a]	RCP-2[a]	Ref.
LBTMO/STO	3.35	220		[62]
$Pr_5Ni_{1.9}Si_3$	8.15	165		[63]
PrNi	6.15	56		[63]
Er_3Ni_2	19.5	507		[64]
TmGa	34.2	485	364	[65]
$GdPd_2Si$	6.0	329		[66]
ErFeSi	23.1	460	365	[67]
LCMO/STO	10.4	298	216	This work
LCMO/LAO	2.88	265	200	This work

[a] Under the field change of 5 T.

IV. CONCLUSION

We reported an anomalous strain effect in LCMO/STO and LCMO/LAO. The MCE and the transition temperatures (i.e., T_C and T_P) for both the tensile and compressive strain at first increase with t (due to strain relaxation) show maximum values at $t \sim 75$ nm and, then, decrease. Such t dependent anomaly of MCE as well as T_C/T_P for both the compressive and tensile strain originates from the simultaneous effect of DE interaction between Mn^{3+} and Mn^{4+} ions and $3d_{x^2-y^2}$ orbital stabilization. Between these two effects, one gets enhanced, while the other one is diminished under the same type of strain relaxation (i.e., either in-plane tensile or in-plane compressive). Therefore, the dominant behavior could be determined by the combined effect of in-plane strain (ϵ_{XX}) and JT distortion (ϵ_{JT}), i.e., the product ($\epsilon_{XX} \times \epsilon_{JT}$). This product decays exponentially and becomes almost zero at ∼75 nm thickness. The decaying of strain induces FM interaction showing the enhanced effect to dominate in the strained film and, just near the strain relaxation point (i.e., at $t \sim 75$ nm), strongest FM interaction is observed. After 75 nm thickness, the diminished effect dominates over the enhanced one to reduce the strength of the FM interaction. The strongest FM interaction has been proven to be the reason behind the maxima in $|\Delta S_{\max}|$ as well in T_C and T_P. It is observed that the variation of $|\Delta S_{\max}|$ follows the Lorentz function with the maximum value at $t \sim 66 \pm 5$ nm for both LCMO/LAO and LCMO/STO. This observation can be used to optimize the thickness of the films to obtain larger MCE for the other magnetocaloric materials together with other manganite thin films. Further, it is observed that the T_C and T_P can be varied with varying the thickness, which makes the epitaxial films flexible for use at various operating temperatures.

ACKNOWLEDGMENTS

W.A. acknowledges DST-INSPIRE. M.B. acknowledges support from a Prime Minister Research Fellowship (PMRF) and institute funding from IISER Thiruvananthapuram. The authors acknowledge IISER Thiruvananthapuram institute funding for magnetic measurements.

[1] K. Gschneidner, Jr., V. Pecharsky, A. Pecharsky, and C. Zimm, Recent developments in magnetic refrigeration, in *Materials Science Forum* (Trans Tech Publ, Switzerland, 1999), Vol. 315, pp. 69–76.

[2] Y. Wang, H. Zhang, E. Liu, X. Zhong, K. Tao, M. Wu, C. Xing, Y. Xiao, J. Liu, and Y. Long, Outstanding comprehensive performance of La(Fe,Si)$_{13}$H$_y$/In composite with durable service life for magnetic refrigeration, Adv. Electron. Mater. **4**, 1700636 (2018).

[3] L. Li and M. Yan, Recent progresses in exploring the rare earth based intermetallic compounds for cryogenic magnetic refrigeration, J. Alloys Compd. **823**, 153810 (2020).

[4] T. Gottschall, K. P. Skokov, M. Fries, A. Taubel, I. Radulov, F. Scheibel, D. Benke, S. Riegg, and O. Gutfleisch, Making a cool choice: the materials library of magnetic refrigeration, Adv. Energy Mater. **9**, 1901322 (2019).

[5] A. Kitanovski, Energy applications of magnetocaloric materials, Adv. Energy Mater. **10**, 1903741 (2020).

[6] X. Moya, S. Kar-Narayan, and N. D. Mathur, Caloric materials near ferroic phase transitions, Nat. Mater. **13**, 439 (2014).

[7] X. Moya, E. Defay, V. Heine, and N. D. Mathur, Too cool to work, Nat. Phys. **11**, 202 (2015).

[8] X. Moya and N. Mathur, Caloric materials for cooling and heating, Science **370**, 797 (2020).

[9] V. Franco, J. Blázquez, J. Ipus, J. Law, L. Moreno-Ramírez, and A. Conde, Magnetocaloric effect: From materials research to refrigeration devices, Prog. Mater. Sci. **93**, 112 (2018).

[10] O. Tegus, E. Brück, K. Buschow, and F. De Boer, Transition-metal-based magnetic refrigerants for room-temperature applications, Nature (London) **415**, 150 (2002).

[11] V. K. Pecharsky and K. A. Gschneidner, Jr., Giant Magnetocaloric Effect in Gd$_5$(Si$_2$Ge$_2$), Phys. Rev. Lett. **78**, 4494 (1997).

[12] V. K. Pecharsky and K. A. Gschneidner, Jr., Tunable magnetic regenerator alloys with a giant magnetocaloric effect for magnetic refrigeration from ∼20 to ∼290 K, Appl. Phys. Lett. **70**, 3299 (1997).

[13] H. Wada and Y. Tanabe, Giant magnetocaloric effect of MnAs$_{1-x}$Sb$_x$, Appl. Phys. Lett. **79**, 3302 (2001).

[14] J. Lyubina, U. Hannemann, L. F. Cohen, and M. P. Ryan, Novel La(Fe,Si)$_{13}$/Cu composites for magnetic cooling, Adv. Energy Mater. **2**, 1323 (2012).

[15] J. Lyubina, R. Schäfer, N. Martin, L. Schultz, and O. Gutfleisch, Novel design of La(Fe,Si)$_{13}$ alloys towards high magnetic refrigeration performance, Adv. Mater. **22**, 3735 (2010).

[16] V. Provenzano, A. J. Shapiro, and R. D. Shull, Reduction of hysteresis losses in the magnetic refrigerant Gd$_5$Ge$_2$Si$_2$ by the addition of iron, Nature (London) **429**, 853 (2004).

[17] V. V. Khovaylo, V. V. Rodionova, S. N. Shevyrtalov, and V. Novosad, Magnetocaloric effect in reduced dimensions: Thin films, ribbons, and microwires of Heusler alloys and related compounds, Phys. Status Solidi B **251**, 2104 (2014).

[18] J. H. Belo, A. L. Pires, J. P. Araújo, and A. M. Pereira, Magnetocaloric materials: From micro- to nanoscale, J. Mater. Res. **34**, 134 (2019).

[19] H. Röder, J. Zang, and A. R. Bishop, Lattice Effects in the Colossal-Magnetoresistance Manganites, Phys. Rev. Lett. **76**, 1356 (1996).

[20] S. Jin, M. McCormack, T. Tiefel, and R. Ramesh, Colossal magnetoresistance in La-Ca-Mn-O ferromagnetic thin films, J. Appl. Phys. **76**, 6929 (1994).

[21] E.-M. Choi, T. Maity, A. Kursumovic, P. Lu, Z. Bi, S. Yu, Y. Park, B. Zhu, R. Wu, V. Gopalan *et al.*, Nanoengineering room temperature ferroelectricity into orthorhombic SmMnO$_3$ films, Nat. Commun. **11**, 2207 (2020).

[22] M. Zarifi, P. Kameli, M. Ehsani, H. Ahmadvand, and H. Salamati, Effects of strain on the magnetic and transport properties of the epitaxial La$_{0.5}$Ca$_{0.5}$MnO$_3$ thin films, J. Magn. Magn. Mater. **420**, 33 (2016).

[23] A. Baena, L. Brey, and M. J. Calderón, Effect of strain on the orbital and magnetic ordering of manganite thin films and their interface with an insulator, Phys. Rev. B **83**, 064424 (2011).

[24] A. Mukherjee, W. S. Cole, P. Woodward, M. Randeria, and N. Trivedi, Theory of Strain-Controlled Magnetotransport and Stabilization of the Ferromagnetic Insulating Phase in Manganite Thin Films, Phys. Rev. Lett. **110**, 157201 (2013).

[25] S. Giri, J. MacManus-Driscoll, W. Li, R. Wu, T. Nath, and T. Maity, Strain induced extrinsic magnetocaloric effects in La$_{0.67}$Sr$_{0.33}$MnO$_3$ thin films, controlled by magnetic field, J. Phys. D **52**, 165302 (2019).

[26] X. Moya, L. Hueso, F. Maccherozzi, A. Tovstolytkin, D. Podyalovskii, C. Ducati, L. Phillips, M. Ghidini, O. Hovorka, A. Berger *et al.*, Giant and reversible extrinsic magnetocaloric effects in La$_{0.7}$Ca$_{0.3}$MnO$_3$ films due to strain, Nat. Mater. **12**, 52 (2013).

[27] M.-H. Phan and S.-C. Yu, Review of the magnetocaloric effect in manganite materials, J. Magn. Magn. Mater. **308**, 325 (2007).

[28] J. Amaral, M. Reis, V. Amaral, T. Mendonca, J. Araujo, M. Sa, P. Tavares, and J. Vieira, Magnetocaloric effect in Er- and Eu-substituted ferromagnetic La-Sr manganites, J. Magn. Magn. Mater. **290**, 686 (2005).

[29] Z. Wang, G. Ni, Q. Xu, H. Sang, and Y. Du, Magnetocaloric effect in perovskite manganites La$_{0.7-x}$Nd$_x$Ca$_{0.3}$MnO$_3$ and La$_{0.7}$Ca$_{0.3}$MnO$_3$, J. Appl. Phys. **90**, 5689 (2001).

[30] A. Antonakos, E. Liarokapis, G. Aydogdu, and H.-U. Habermeier, Strain effects on La$_{0.5}$Ca$_{0.5}$MnO$_3$ thin films, Mater. Sci. Eng.: B **144**, 83 (2007).

[31] G. Aydogdu, Y. Kuru, and H.-U. Habermeier, Novel electronic and magnetic properties of La$_{0.5}$Ca$_{0.5}$MnO$_3$ films deposited on (1 1 1) SrTiO$_3$ substrates, J. Cryst. Growth **310**, 4521 (2008).

[32] J. Zhang, H. Tanaka, T. Kanki, and T. Kawai, Anomalous strain effect on magnetic properties of La$_{1-x}$Ba$_x$MnO$_3$ epitaxial thin films, Surf. Interface Anal. **32**, 62 (2001).

[33] F. Razavi, G. Gross, H.-U. Habermeier, O. Lebedev, S. Amelinckx, G. Van Tendeloo, and A. Vigliante, Epitaxial strain induced metal insulator transition in La$_{0.9}$Sr$_{0.1}$MnO$_3$ and La$_{0.88}$Sr$_{0.1}$MnO$_3$ thin films, Appl. Phys. Lett. **76**, 155 (2000).

[34] M. Evangelisti, O. Roubeau, E. Palacios, A. Camón, T. N. Hooper, E. K. Brechin, and J. J. Alonso, Cryogenic magnetocaloric effect in a ferromagnetic molecular dimer, Angew. Chem., Int. Ed. **50**, 6606 (2011).

[35] M. Manoli, R. D. Johnstone, S. Parsons, M. Murrie, M. Affronte, M. Evangelisti, and E. K. Brechin, A ferromagnetic mixed-valent Mn supertetrahedron: Towards low-temperature magnetic refrigeration with molecular clusters, Angew. Chem. **119**, 4540 (2007).

[36] M. Evangelisti and E. K. Brechin, Recipes for enhanced molecular cooling, Dalton Trans. **39**, 4672 (2010).

[37] G. Q. Gong, A. Gupta, G. Xiao, P. Lecoeur, and T. R. McGuire, Perovskite oxide superlattices: Magnetotransport and magnetic properties, Phys. Rev. B **54**, R3742(R) (1996).

[38] W. Prellier, A. Haghiri-Gosnet, B. Mercey, P. Lecoeur, M. Hervieu, C. Simon, and B. Raveau, Spectacular decrease of the melting magnetic field in the charge-ordered state of $Pr_{0.5}Ca_{0.5}MnO_3$ films under tensile strain, Appl. Phys. Lett. **77**, 1023 (2000).

[39] T. Kanki, H. Tanaka, and T. Kawai, Anomalous strain effect in $La_{0.8}Ba_{0.2}MnO_3$ epitaxial thin film: role of the orbital degree of freedom in stabilizing ferromagnetism, Phys. Rev. B **64**, 224418 (2001).

[40] J. Zhang, H. Tanaka, T. Kanki, J.-H. Choi, and T. Kawai, Strain effect and the phase diagram of $La_{1-x}Ba_xMnO_3$ thin films, Phys. Rev. B **64**, 184404 (2001).

[41] X. Zhang, J. Tejada, Y. Xin, G. Sun, K. Wong, and X. Bohigas, Magnetocaloric effect in $La_{0.67}Ca_{0.33}MnO_\delta$ and $La_{0.60}Y_{0.07}Ca_{0.33}MnO_\delta$ bulk materials, Appl. Phys. Lett. **69**, 3596 (1996).

[42] A. Chaturvedi, S. Stefanoski, M.-H. Phan, G. S. Nolas, and H. Srikanth, Table-like magnetocaloric effect and enhanced refrigerant capacity in $Eu_8Ga_{16}Ge_{30}$-EuO composite materials, Appl. Phys. Lett. **99**, 162513 (2011).

[43] N. K. Singh, S. Agarwal, K. G. Suresh, R. Nirmala, A. K. Nigam, and S. K. Malik, Anomalous magnetocaloric effect and magnetoresistance in $Ho(Ni,Fe)_2$ compounds, Phys. Rev. B **72**, 014452 (2005).

[44] R. Rao, D. Lavric, T. Nath, C. Eom, L. Wu, and F. Tsui, Effects of film thickness and lattice mismatch on strain states and magnetic properties of $La_{0.8}Ca_{0.2}MnO_3$ thin films, J. Appl. Phys. **85**, 4794 (1999).

[45] T. D. Thanh, N. T. Dung, N. Van Dang, L. V. Bau, H.-G. Piao, T. L. Phan, P. D. Huyen Yen, K. X. Hau, D.-H. Kim, and S.-C. Yu, Tuning the magnetic phase transition and the magnetocaloric properties of $La_{0.7}Ca_{0.3}MnO_3$ compounds through Sm-doping, AIP Adv. **8**, 056419 (2018).

[46] S. Banerjee, On a generalised approach to first and second order magnetic transitions, Phys. Lett. **12**, 16 (1964).

[47] S. Xi, W. Lu, and Y. Sun, Magnetic properties and magnetocaloric effect of $La_{0.8}Ca_{0.2}MnO_3$ nanoparticles tuned by particle size, J. Appl. Phys. **111**, 063922 (2012).

[48] B. Martinez, X. Obradors, L. Balcells, A. Rouanet, and C. Monty, Low Temperature Surface Spin-Glass Transition in γ-Fe_2O_3 Nanoparticles, Phys. Rev. Lett. **80**, 181 (1998).

[49] S. Xi, W. Lu, H. Wu, P. Tong, and Y. Sun, Surface spin-glass, large surface anisotropy, and depression of magnetocaloric effect in $La_{0.8}Ca_{0.2}MnO_3$ nanoparticles, J. Appl. Phys. **112**, 123903 (2012).

[50] Y. Fu, Grain-boundary effects on the electrical resistivity and the ferromagnetic transition temperature of $La_{0.8}Ca_{0.2}MnO_3$, Appl. Phys. Lett. **77**, 118 (2000).

[51] R. Zhang and R. F. Willis, Thickness-Dependent Curie Temperatures of Ultrathin Magnetic Films: Effect of the Range of Spin-Spin Interactions, Phys. Rev. Lett. **86**, 2665 (2001).

[52] E. Almahmoud, I. Kornev, and L. Bellaiche, Dependence of Curie temperature on the thickness of an ultrathin ferroelectric film, Phys. Rev. B **81**, 064105 (2010).

[53] X. R. Wang, C. J. Li, W. Lü, T. Paudel, D. Leusink, M. Hoek, N. Poccia, A. Vailionis, T. Venkatesan, J. Coey *et al.*, Imaging and control of ferromagnetism in $LaMnO_3/SrTiO_3$ heterostructures, Science **349**, 716 (2015).

[54] J. Coey, M. Viret, and S. Von Molnar, Mixed-valence manganites, Adv. Phys. **48**, 167 (1999).

[55] J. B. Goodenough, Theory of the role of covalence in the perovskite-type manganites $[La,M(II)]MnO_3$, Phys. Rev. **100**, 564 (1955).

[56] P. Cox, The electronic structure of transition metal oxides and chalcogenides, in *Physics and Chemistry of Low-Dimensional Inorganic Conductors* (Springer, Boston, MA, 1996), pp. 255–270.

[57] H. B. Khlifa, F. Ayadi, R. M'nassri, W. Cheikhrouhou-Koubaa, G. Schmerber, and A. Cheikhrouhou, Screening of the synthesis route on the structural, magnetic and magnetocaloric properties of $La_{0.6}Ca_{0.2}Ba_{0.2}MnO_3$ manganite: A comparison between solid-solid state process and a combination polyol process and spark plasma sintering, J. Alloys Compd. **712**, 451 (2017).

[58] J. Amaral and V. Amaral, On estimating the magnetocaloric effect from magnetization measurements, J. Magn. Magn. Mater. **322**, 1552 (2010).

[59] L. A. Burrola Gándara, L. Vázquez Zubiate, D. M. Carrillo Flores, J. T. Elizalde Galindo, C. Ornelas, and M. Ramos, Tuning magnetic entropy change and relative cooling power in $La_{0.7}Ca_{0.23}Sr_{0.07}MnO_3$ electrospun nanofibers, Nanomaterials **10**, 435 (2020).

[60] L. Marín, L. A. Rodríguez, C. Mageín, E. Snoeck, R. Arras, I. Lucas, L. Morellon, P. A. Algarabel, J. M. De Teresa, and M. R. Ibarra, Observation of the strain induced magnetic phase segregation in manganite thin films, Nano Lett. **15**, 492 (2015).

[61] M. Khlifi, A. Tozri, M. Bejar, E. Dhahri, and E. Hlil, Effect of calcium deficiency on the critical behavior near the paramagnetic to ferromagnetic phase transition temperature in $La_{0.8}Ca_{0.2}MnO_3$ oxides, J. Magn. Magn. Mater. **324**, 2142 (2012).

[62] M. Oumezzine, A. C. Galca, I. Pasuk, C. F. Chirila, A. Leca, V. Kuncser, L. C. Tanase, A. Kuncser, C. Ghica, and M. Oumezzine, Structural, magnetic and magnetocaloric effects in epitaxial $La_{0.67}Ba_{0.33}Ti_{0.02}Mn_{0.98}O_3$ ferromagnetic thin films grown on 001-oriented $SrTiO_3$ substrates, Dalton Trans. **45**, 15034 (2016).

[63] A. O. Pecharsky, Y. Mozharivskyj, K. W. Dennis, K. A. Gschneidner, Jr., R. W. McCallum, G. J. Miller, and V. K. Pecharsky, Preparation, crystal structure, heat capacity, magnetism, and the magnetocaloric effect of $Pr_5Ni_{1.9}Si_3$ and PrNi, Phys. Rev. B **68**, 134452 (2003).

[64] Q. Dong, J. Chen, J. Shen, J. Sun, and B. Shen, Magnetic properties and magnetocaloric effects in R_3Ni_2 (R = Ho and Er) compounds, Appl. Phys. Lett. **99**, 132504 (2011).

[65] Z.-J. Mo, J. Shen, L.-Q. Yan, C.-C. Tang, J. Lin, J.-F. Wu, J.-R. Sun, L.-C. Wang, X.-Q. Zheng, and B.-G. Shen, Low field induced giant magnetocaloric effect in TmGa compound, Appl. Phys. Lett. **103**, 052409 (2013).

[66] R. Rawat and I. Das, Magnetocaloric and magnetoresistance studies of $GdPd_2Si$, J. Phys.: Condens. Matter **13**, L57 (2001).

[67] H. Zhang, B. Shen, Z. Xu, J. Shen, F. Hu, J. Sun, and Y. Long, Large reversible magnetocaloric effects in ErFeSi compound under low magnetic field change around liquid hydrogen temperature, Appl. Phys. Lett. **102**, 092401 (2013).

[68] V. Chaudhary and R. V. Ramanujan, High relative cooling power in a multiphase magnetocaloric FeNiB alloy, IEEE Magn. Lett. **6**, 1 (2015).

[69] M. Wood and W. Potter, General analysis of magnetic refrigeration and its optimization using a new concept: maximization of refrigerant capacity, Cryogenics **25**, 667 (1985).

[70] K. Gschneidner, Jr. and V. K. Pecharsky, Magnetocaloric materials, Annu. Rev. Mater. Sci. **30**, 387 (2000).

[71] V. Zverev, A. Tishin, and M. Kuz'Min, The maximum possible magnetocaloric ΔT effect, J. Appl. Phys. **107**, 043907 (2010).

[72] R. Caballero-Flores, V. Franco, A. Conde, K. Knipling, and M. Willard, Optimization of the refrigerant capacity in multiphase magnetocaloric materials, Appl. Phys. Lett. **98**, 102505 (2011).

[73] L. Li, O. Niehaus, M. Kersting, and R. Pöttgen, Reversible table-like magnetocaloric effect in Eu_4PdMg over a very large temperature span, Appl. Phys. Lett. **104**, 092416 (2014).